Application of dynamical eikonal approximation in elastic scattering reaction within 10–60 MeV/nucleon*

Xiao-Yan Yun (韵小艳)[1] Dan-Yang Pang (庞丹阳)[2] Yi-Ping Xu (许祎萍)[3†]

[1]College of Physics and Optoelectronics, Taiyuan University of Technology, Taiyuan 030024, China
[2]School of Physics, Beihang University, Beijing 100191, China
[3]School of Nuclear Science and Engineering, North China Electric Power University, Beijing 102206, China

Abstract: We study the application of the dynamical eikonal approximation (DEA) to elastic scattering for Coulomb-dominated reactions at low energy. Our test case consists of elastic scattering for ^{8}B, ^{9}C, and ^{11}Be on ^{208}Pb at 21.3, 25.2 and 12.7 MeV/nucleon, respectively. We introduce an empirical correction to the DEA method to account for Coulomb deflection, which significantly improves the description of elastic scattering of weakly-bound nuclei on a heavy target. The angular distributions of elastic scattering obtained using the empirical correction show good agreement with experimental data down to approximately 10 MeV/nucleon. Furthermore, we study the the effect of relativistic kinematics corrections on the angular distributions of elastic scattering at incident energies between 20 and 60 MeV/nucleon. The results show that relativistic kinematics corrections are crucial for describing the angular distributions of elastic scattering as low as approximately 40 MeV/nucleon.

Keywords: elastic scattering, empirical correction, relativistic kinematics correction

DOI: 10.1088/1674-1137/ade127 **CSTR:** 32044.14.ChinesePhysicsC.49094103

I. INTRODUCTION

With the development of radioactive ion beam physics in the mid-1980s, Isotope Separator On-Line (ISOL) facilities have been able to produce an increasing number of intermediate and high-energy beams, as well as short-lived nuclides. The number of observed nuclides has soared from approximately 300 to over 3000, while the number of theoretically predicted nuclides is estimated to be as high as 8000-10000, the vast majority of which are unstable. The study of exotic nuclei that lie far from the β stability line has emerged as one of the primary objectives in astrophysics. This research is intrinsically linked to the synthesis of elements and the evolution of celestial bodies following the Big Bang. Numerous novel phenomena have been uncovered in unstable nuclei. For example, the existence of neutron halo or neutron skin in some nuclei [1–3], emergence of new magic numbers [4–7], and shape co-existence [8, 9] have been discovered. New phenomena continue to provide challenges to nuclear theory. These exotic nuclear structures also manifest themselves in reactions induced by radioactive nuclei. Elastic scattering induced by weakly-bound nuclei is of paramount importance, as it contains crucial information about the exotic structure and reaction mechanism of these weakly-bound nuclei [10]. One particularly notable phenomenon is the significant reduction of the Coulomb-nuclear interference peak in the elastic scattering angular distributions of weakly-bound nuclei, such as ^{6}He and ^{11}Be. This reduction has been found to be caused by coupling effects from breakup reaction channels [11–16].

Several cutting-edge facilities, such as HIE-ISOLDE at CERN, are already operational or will soon provide radioactive ion beams (RIBs) at energies as low as 10 MeV/nucleon, necessitating robust theoretical support for experiments in this low-energy region. Recently, the High Intensity Heavy-ion Accelerator Facility (HIAF) has been established in Huizhou, Guangdong Province. This advanced facility can deliver high-intensity beams of both stable and radioactive ions, covering an extensive energy range from MeV/u to GeV/u. HIAF is expected to facilitate a wide array of elastic scattering experiments across this broad energy spectrum. Therefore, a reaction method applicable across a broad energy range, capable of effectively handling elastic scattering of weakly-bound nuclei, and featuring high numerical stability and computational efficiency is essential.

Some theories have been proposed to achieve this goal. Among them, the Continuum Discretized Coupled-Channels (CDCC) method has proven to be a highly suc-

Received 24 April 2025; Accepted 4 June 2025; Published online 5 June 2025

* Supported by the National Natural Science Foundation of China (12205098, U2067205) and the Fundamental Research Funds for the Central Universities (2025MS063)

† E-mail: E-mail: xuyp_snse@ncepu.edu.cn

cessful tool for describing reactions induced by weakly-bound systems [17–20]. As CDCC treats the collision in a fully quantum mechanical manner, it can be computationally demanding. Additionally, it faces challenges in achieving convergent results in the low-energy region, while relativistic effects must be considered in the high-energy region [21].

Dynamical Eikonal Approximation (DEA) relies on the eikonal approximation, which assumes that the projectile-target interaction occurs along a straight line [22, 23]. Based on this assumption, the wave function can be factorized into a plane wave multiplied by a function that varies smoothly with the projectile-target relative coordinate. This factorization allows us to perform reaction calculations more efficiently, reducing the computational time compared to the CDCC method. Moreover, the DEA method is an improvement over the traditional eikonal approximation, as it fully accounts for the dynamical effects of projectile excitation. This aviods the divergence issue in the integral over impact parameter b during cross-section calculations within the eikonal approximation. In previous studies, a detailed comparison was conducted between the CDCC and DEA methods for the breakup of the one-neutron halo nucleus ^{15}C on ^{208}Pb at an incident energy of 68 MeV/nucleon [24]. The results from both methods are in excellent agreement. However, the DEA method fails to reproduce the CDCC results at 20 MeV/nucleon, as the eikonal approximation becomes invalid at such low energies, which stems from the Coulomb deflection. At low energies, it significantly distorts the projectile-target relative motion from a pure plane wave. Therefore, it is crucial to find a way to correct it for the low-energy case in DEA. Recent results have shown that an empirical correction can markedly enhance the description of breakup reactions involving neutron-rich projectiles on heavy targets, down to incident energies of 20 MeV/nucleon [25]. The empirical correction replaces the impact parameter with the distance of closest approach of the corresponding classical trajectory. The excellent results obtained for neutron-rich nuclei lead us to consider the extension of the correction to study the application of proton-rich nuclei. However, the feasibility of applying the DEA to the elastic scattering of proton-rich nuclei on heavy targets at these energies remains unexplored.

This study examined three specific reactions: ^{8}B, ^{9}C and ^{11}Be impinging on ^{208}Pb at incident energies of 21.3, 25.2, and 12.7 MeV/nucleon, respectively. We applied the DEA method to elastic scattering reactions at incident energies of several tens of MeV/nucleon with the empirical and relativistic kinematics corrections. This energy range is typically considered to be one where relativistic effects are negligible. The aim of this study was to investigate the feasibility of extending the DEA method to a wide energy range.

The remainder of this paper is organized as follows. The theoretical framework of the DEA, empirical correction, and relativistic kinematics correction are introduced in Section II. The results of empirical and relativistic kinematics corrections with and without taking into account such corrections are shown in Section III. Finally, a summary of this paper is given in Section IV.

II. THEORETICAL FRAMEWORK

A. Dynamical eikonal approximation

We consider a collision between a two-body projectile (P) and a structureless target (T) with mass m_T and charge $Z_T e$. The two-body projectile consists of a structureless core (c) with mass m_c and charge $Z_c e$ and a fragment (f) with mass m_f and charge $Z_f e$. The projectile is described by the internal Hamiltonian

$$H_0 = -\frac{\hbar^2}{2\mu_{cf}} \triangle_{\boldsymbol{r}} + V_{cf}(\boldsymbol{r}), \tag{1}$$

where $\mu_{cf} = \dfrac{m_f m_c}{m_f + m_c}$ is the c-f reduced mass of the projectile, and $\boldsymbol{r}$ is the relative coordinate of the fragment to the core. H_0 is composed of the kinetic energy operator for the relative motion between core and fragment and of the core-fragment interaction potential V_{cf}. The potential V_{cf} contains an angular-momentum-dependent central term (including a Coulomb interaction) and spin-orbit term involving the fragment spin, where the spin of the core is neglected.

With this two-body description for the projectile, the P-T collision reduces to a three-body problem whose Hamiltonian (H) reads

$$H = \hat{T}_{PT} + H_0 + V_{cT} + V_{fT}, \tag{2}$$

where $\hat{T}_{PT}$ is the kinetic energy operator of projectile-target relative motion, and V_{cT} and V_{fT} are the core-target and fragment-target system interactions, respectively.

To study the reactions of projectile (P) on target (T), we need to solve the three-body Schrödinger equation

$$\left[\hat{T}_{PT} + H_0 + V_{cT} + V_{fT}\right] \Psi(\boldsymbol{R}_{PT}, \boldsymbol{r}) = E\Psi(\boldsymbol{R}_{PT}, \boldsymbol{r}), \tag{3}$$

where $\Psi(\boldsymbol{R}_{PT}, \boldsymbol{r})$ is the three-body wave function, E is the total energy of the system, and $\boldsymbol{R}_{PT}$ is the coordinate of the projectile with respect to the target. In the DEA method, the resulting three-body Schrödinger equation is solved using the eikonal ansatz for the wave function

$$\Psi(\boldsymbol{R}_{PT}, \boldsymbol{r}) = \mathrm{e}^{\mathrm{i}KZ} \widehat{\Psi}(\boldsymbol{R}_{PT}, \boldsymbol{r}), \tag{4}$$

where K is wave number, which is related to the total en-

ergy E.

At high energies, one expects a weak dependence on $\boldsymbol{R}_{PT}$ of $\widehat{\Psi}$. Using the factorization of Eq. (4) in Eq. (3) and neglecting second-order derivatives of $\widehat{\Psi}$ that are small at high velocities, we obtain

$$\mathrm{i}\hbar v\frac{\partial}{\partial Z}\widehat{\Psi}(\boldsymbol{b},Z,\boldsymbol{r}) = [(H_0 - E_0) + V_{cT} + V_{fT}]\widehat{\Psi}(\boldsymbol{b},Z,\boldsymbol{r}), \quad (5)$$

where Z represents the longitudinal components of $\boldsymbol{R}_{PT}$, the vector $\boldsymbol{b} = (b,\phi)$ represents the transverse part of $\boldsymbol{R}_{PT}$, v is the relative velocity of projectile and target, and E_0 corresponds to the projectile ground state of energy. In the standard eikonal implementation, the adiabatic approximation is performed to solve Eq. (5). That approximation corresponds to neglecting the excitation energy of the projectile compared to the beam energy. In DEA, no such adiabatic approximation is made, and Eq. (5) is solved numerically for each impact parameter $\boldsymbol{b}$, imposing the initial condition. Initially, the projectile is in its ground state $n_0l_0j_0$ of energy E_0 and has an initial P-T relative momentum $\hbar K_0$, where j_0 is the total angular momentum. This results from the coupling of the orbital angular momentum l_0 and spin of the fragment, where m_0 is its projection. ϕ corresponds to the projectile ground state wave function.

$$\widehat{\Psi}^{(m_0)}(\boldsymbol{b},t\to-\infty,\boldsymbol{r}) = \phi_{l_0j_0m_0}(E_0,\boldsymbol{r}), \quad (6)$$

where the variable $t(Z = vt)$ is linked to the longitudinal part of $\boldsymbol{R}_{PT}$.

Let $\widehat{\Psi}^{(m_0)}(b,t,\boldsymbol{r})$ be a particular solution (to the particular orientation $\boldsymbol{b}$=(b,ϕ=0)) of Eq. (5) corresponding to the initial condition $\widehat{\Psi}^{(m_0)}(\boldsymbol{b},t\to-\infty,\boldsymbol{r}) = \phi_{l_0j_0m_0}(\boldsymbol{r})$. b is the impact parameter related to a classical trajectory, whereas in Eq. 6, $\boldsymbol{b}$ is the transverse part of a quantal coordinate.

The elastic scattering differential cross-section can be deduced from the wave function (see Ref. [26] for more details)

$$\frac{\mathrm{d}\sigma}{\mathrm{d}\Omega_{el}} \propto \langle\phi_{l_0j_0m_0}(E_0,\boldsymbol{r})|\widehat{\Psi}^{(m_0)}(\boldsymbol{R},\boldsymbol{r})\rangle, \quad (7)$$

B. Empirical correction

As previously discussed, the DEA method is based on the eikonal approximation, which assumes that the interaction between the projectile and target occurs along a straight line [22, 23]. However, in reality, the trajectory deviates from a straight line due to the deflection caused by the interaction with the target. At sufficiently high energies, the assumption of straight-line trajectories becomes more valid, as the deflection of the projectile by the target can be considered negligible. The eikonal approximation becomes invalid at low energies, which stems from the Coulomb deflection. At low energies, the projectile-target relative motion is significantly distorted from a pure plane wave.

Fukui *et al*. discovered that DEA no longer aligns with the CDCC calculation for the breakup of ^{15}C on ^{208}Pb at 20 MeV/nucleon. They observed that the discrepancies between DEA and CDCC are not only in the magnitude of the angular distributions but also in the angular distributions. Specifically, the oscillatory pattern of DEA is shifted towards more forward angles compared to the CDCC calculation. To pinpoint the source of this discrepancy, they analyzed the contribution of each projectile-target relative angular momentum L to the total breakup cross-section. They found that the DEA method tends to favor larger L values compared to the full CDCC calculation. To address this issue, they replaced the transverse component of the projectile-target relative coordinate b with the empirical value. For a collision dominated by the repulsive Coulomb interaction, that distance will be larger than b. The distance of closest approach b' can be derived analytically [27, 28]:

$$b' = \frac{\eta_0}{K_0} + \sqrt{\frac{\eta_0^2}{K_0^2} + b^2}, \quad (8)$$

where η is the Sommerfeld parameter, $\eta_0 = \dfrac{Z_P Z_T e^2 \mu_{PT}}{\hbar^2 K_0}$, Z_P and Z_T are the charges of the projectile and target, respectively, and K_0 is the wave number for the initial projectile-target, which is related to the total energy $E = \hbar^2K_0/2\mu_{PT} + E_0$. Ref. [25] showed that this simple empirical correction could significantlyimprove the description of breakup for neutron-rich nuclei on heavy targets at approximately 20 MeV/nucleon.

C. Relativistic kinematics correction

For high-energy reactions that have transcended the nonrelativistic energy regime, the influence of relativistic effects can be taken into account. To provide a reliable theoretical interpretation of experimental data, it is imperative to develop a theoretical method of nuclear reactions that incorporates relativistic effects. This section introduces the relativistic kinematics corrections. When addressing relativity in nuclear reactions, several key aspects must be considered. For instance, the Schrödinger equation is not strictly valid in a relativistic context; thus, at least some re-interpolation of the nuclear optical potential is necessary [21]. Additionally, the parameters of reaction kinematics, including atomic masses and incident energies, require modification to account for relativistic effects. The latter aspect is rather simple, but it has been found to be important for some cases. In this paper, we

study the latter aspect. The velocity v of the projectile, which is utilized to solve the time-dependent Schrödinger equation in Eq. (5), is calculated using the relativistic formula

$$\frac{v}{c} = \sqrt{1 - \frac{1}{\left(1 + \frac{T_P}{m_P c^2}\right)^2}}, \tag{9}$$

where T_P is the initial kinetic energy of the projectile, and m_P is the mass of the projectile.

We also use the relativistic kinematics correction method proposed by Satchler [29]. Define γ_i^L as

$$\gamma_i^L = \frac{T_P^L}{m_P c^2} + 1, \tag{10}$$

where T_P^L is the incident energy per nucleon in the laboratory system. γ_P corresponds to the projectile:

$$\gamma_P = \frac{x_P + \gamma_i^L}{\sqrt{1 + x_P^2 + 2x_P\gamma_i^L}}, \tag{11}$$

γ_T corresponds to the target nucleus:

$$\gamma_T = \frac{x_T + \gamma_i^L}{\sqrt{1 + x_T^2 + 2x_T\gamma_i^L}}, \tag{12}$$

where $x_P = \frac{m_P c^2}{m_T c^2}$ and $x_T = \frac{m_T c^2}{m_P c^2}$. Then, the masses of the projectile and target nuclei after relativistic correction are $m'_P = \gamma_P m_P$ and $m'_T = \gamma_T m_T$, respectively, and the reduced mass of the projectile-target system becomes

$$\mu_{PT} = \frac{\frac{x_P + \gamma_i^L}{\sqrt{1 + x_P^2 + 2x_P\gamma_i^L}} m_P \frac{x_T + \gamma_i^L}{\sqrt{1 + x_T^2 + 2x_T\gamma_i^L}} m_T}{\frac{x_P + \gamma_i^L}{\sqrt{1 + x_P^2 + 2x_P\gamma_i^L}} m_P + \frac{x_T + \gamma_i^L}{\sqrt{1 + x_T^2 + 2x_T\gamma_i^L}} m_T}. \tag{13}$$

D. Inputs to the reaction method

We analyze the elastic scattering induced by ^{8}B,^{9}C, and ^{11}Be on ^{208}Pb at 21.3, 25.2 and 12.7 MeV/nucleon, respectively. The nucleus ^{8}B is usually considered as the archetypical one-proton halo nucleus, with a valence proton and ^{7}Be core. The spectrum of ^{8}B includes only one bound state with $J^\pi = 2^+$, which is obtained from the coupling of a $0p_{3/2}$ proton with the $3/2^-$ spin of the ground state of the ^{7}Be. It is bound by a mere 137 keV in regard to the one-proton separation. In this work, we use the description of ^{8}B developed by Bertsch in Ref. [30]. ^{9}C is seen as a valence proton (in the $0p_{3/2}$ orbital) and a ^{8}B core. We use the description of ^{9}C from Ref. [16]. ^{11}Be is seen as an inert ^{10}B core in its 0^+ ground state, to which a neutron is bound by 0.5 MeV in the $1s_{1/2}$ orbit. The ^{11}Be description in this paper corresponds to a simplified version in Ref. [31, 32]. For computational reasons, we use a simple method for ^{8}B, ^{9}C, and ^{11}Be, where the spin and internal structure of the core are neglected.

The DEA equation is solved with the algorithm presented in Refs. [26, 33], and the wave function is expanded over a mesh on the unit sphere containing $N_\theta \times N_\varphi$ points. We go up to 10×19 points for these cases. The radial mesh is quasi-uniform, contains N_r=800 points, and extends up to r_{N_r} = 800 fm. These calculations are performed for impact parameters b= 0–150 fm with a discretization step that varies between 0.25 and 5 fm. As explained in Ref. [34], the angular distributions of elastic scattering are obtained with an extrapolation up to $b_{\max}$=800 fm.

CDCC calculations are performed using FRESCO code. Proton-^{7}Be(^{8}B) relative orbital angular momentum up to $l_{\max}$=3 was included with all couplings up to multipolarity $\lambda_{\max}$=3. The continuum was discretized up to a maximum Proton-^{7}Be relative energy of $E_{\max}$=15.3 MeV, corresponding to $k_{\max}$=0.8 fm^{-1}, divided into eight equally-spaced bins of width 0.1 fm^{-1}, giving a total of 32 bins. The continuum states of the proton-^{8}B(^{9}C case) system were discretized into nine bins up to a maximum excitation energy of $E_{\max}$ = 18.7 MeV. $k_{\max}$ = 0.9 fm^{-1} was discretized into eight equally-spaced bins of width 0.1 fm^{-1}, giving a total of 36 bins. Proton-^{8}B relative orbital angular momentum reaches up to $l_{\max}$= 3 and $\lambda_{\max}$=3 multipoles in the expansion of the coupling potentials. The continuum states of the neutron-^{10}Be(^{11}Be case) system were discretized into nine bins up to a maximum excitation energy of $E_{\max}$=17.5 MeV, corresponding to $k_{\max}$ = 0.9 fm^{-1}. The proton-^{8}B relative orbital angular momentum up to $l_{\max}$ = 5 was included with all couplings up to a maximum multipolarity $\lambda_{\max}$ = 5. Convergence of elastic scattering cross-sections were ensured by using an increased model space.

In these calculations, the core-target interactions, V_{cT}, are obtained with the systematic single-folding method of nucleus-nucleus potentials [21], which accounts well for the nucleus-nucleus elastic scattering not only for stable nuclei but also for some unstable nuclei within the energy range of approximately 10−100 MeV/nucleon. The fragment-target interactions, V_{fT}, are taken from the CH89 systematics [35]. The Coulomb potentials for the c-T, f-T, and c-f systems are calculated with a uniform distribution of a charge sphere with radius R_C=$r_C(A_T^{1/3}$+$A_c^{1/3})$, $r_C(A_T^{1/3})$, and $r_C(A_c^{1/3})$, respectively, where r_C = 1.25 fm, and A_T and A_c are the mass numbers of the target and core nuclei, respectively.

III. RESULTS AND DISCUSSION

Figures 1 and 2 show the analysis of ^{8}B and ^{9}C on ^{208}Pb at low energies (21.3 and 25.2 MeV/nucleon, respectively). These figures display the angular distributions of elastic scattering (ratio to Rutherford, σ/σ_R) as a function of the center of mass of scattering angles, $\theta_{\rm c.m.}$. The pink dotted curves represent the results of DEA with empirical correction (labeled as "Corr"), while the green dash-dotted curves correspond to the results of DEA without empirical correction (labeled as "NoCorr"). The blue dashed curves correspond to the results of the CDCC method. As shown in Fig. 1, the results of the CDCC and experimental data agree very well with each other. The results of the DEA and experimental data no longer agree with each other at 21.3 MeV/nucleon. We see that not only do the DEA and CDCC differ in magnitude, but also DEA oscillatory pattern is shifted to a forward angle compared to the CDCC. When the empirical correction is switched on, the agreement between the two methods is good. The results confirm that the empirical correction is very effective. This significantly improves the agreement with CDCC method. The results in Fig. 2 are very similar to those in Fig. 1 for ^{8}B. Note that the results of DEA using the correction seem to show good agreement with the CDCC results and experimental data.

To further verify the applicability of the empirical correction to lower-energy reactions, we study the case of ^{11}Be on a lead target at 12.7 MeV/nucleon. As shown in Fig. 3, compared to the case at approximately 20 MeV/nucleon, the discrepancy between the results of the DEA and CDCC becomes more pronounced at 12.7 MeV/nucleon. Nevertheless, the DEA still successfully reproduces the angular distributions obtained from the CDCC. The results of these calculation suggest that DEA could extend its range of validity down to 10 MeV/nucleon in Coulomb-dominated collisions.

The difference observed between the DEA and experimental data at low energy is related to the root: the lack of Coulomb deflection in the DEA. Based on the eikonal approximation, the DEA presumes that the incoming plane-wave motion of the projectile remains largely unperturbed by its interaction with the target. Nevertheless, the results show that the lack of Coulomb deflection for the DEA calculations can be efficiently corrected by the empirical correction (see the curve labeled "Corr"). While efficient, the empirical correction is not perfect. A slight shift of the oscillatory pattern to larger scattering angles can be seen compared to the experimental data. However, its oscillatory pattern is now in phase with experimental data. This correction provides a simple and effective way to account for Coulomb deflection in the DEA method. In the following calculations, the empirical correction is included.

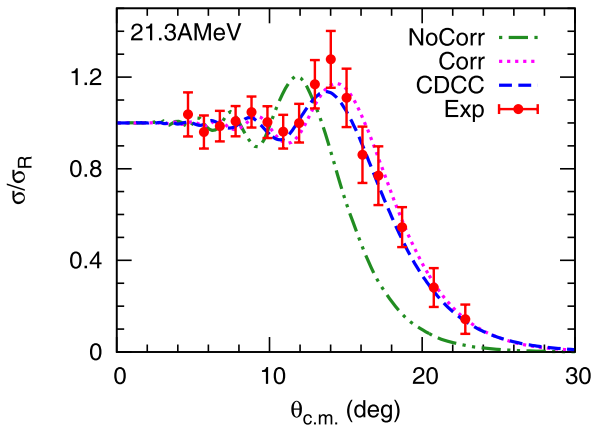

Fig. 1. (color online) Comparison between theoretical and experimental (red circle) angular distributions for the elastic scattering of ^{8}B on ^{208}Pb at 21.3 MeV/nucleon (see text for details). The experimental data are from Ref. [36].

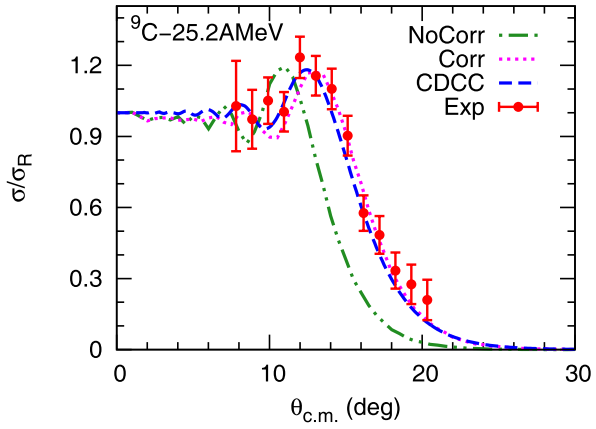

Fig. 2. (color online) Comparison between theoretical and experimental (red circle) angular distributions for the elastic scattering of ^{9}C on ^{208}Pb at 25.2 MeV/nucleon (see text for details). The experimental data are from Ref. [16].

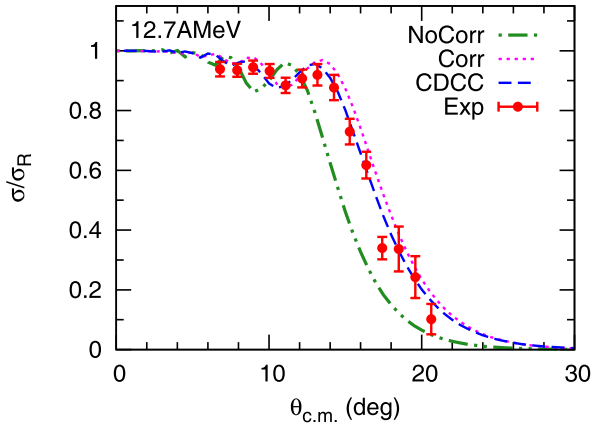

Fig. 3. (color online) Comparison between theoretical and experimental (red circle) angular distributions for the elastic scattering of ^{11}Be on ^{208}Pb at 12.7 MeV/nucleon (see text for details). The experimental data are from Ref. [15].

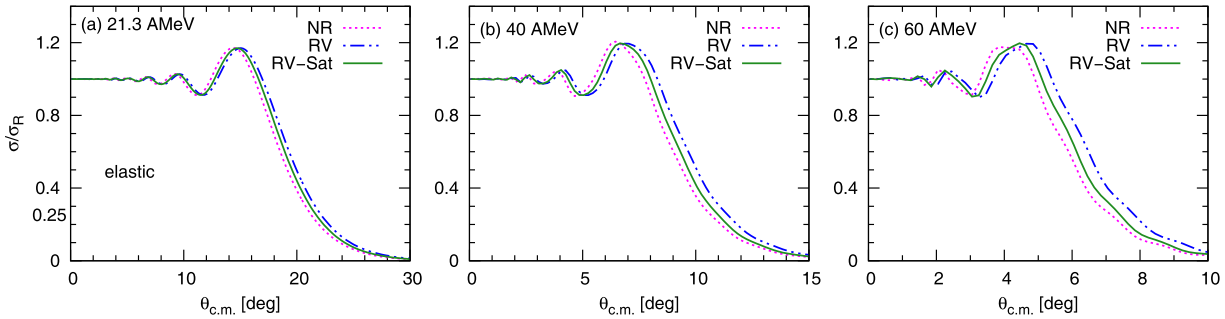

Fig. 4. (color online) Effect of relativistic corrections on angular distributions of elastic scattering for ^{8}B on ^{208}Pb at different incident energies. The dotted, dashed-double-dotted, and solid curves, labeled as "NR", "RV" and "RV-Sat", respectively, correspond to results without taking into account the relativistic corrections, taking into account the relativistic correction of the velocity, and taking into account velocity and Satchler's relativistic correction.

The calculations in Figs. 1, 2, and 3 are performed within the nonrelativistic framework. However, it is well known that at sufficiently high incident energies, relativistic effects must be taken into account. We investigate reactions with incident energies in the range of several tens of MeV/nucleon. At these energy levels, relativistic effects may start to become significant. Consequently, we incorporate relativistic kinematics corrections into the subsequent calculations to account for this influence.

To study how the importance of the relativistic corrections evolves with the incident energy of the projectile, we study the elastic scattering reaction of ^{8}B on ^{208}Pb at 20, 40, and 60 MeV/nucleon. The results are shown in Fig. 4. The pink dotted curves represent the results obtained without considering relativistic corrections. The blue dashed-double-dotted curves represent the results with the inclusion of the relativistic correction for velocity (Eq. 9), marked as "RV". The green curves correspond to the results incorporating both velocity and Satchler's relativistic corrections, labeled as "RV-Sat". As expected, the effect of relativistic corrections is minimal at lower incident energies. It is evident that the significance of relativistic corrections becomes apparent at 40 MeV/nucleon and increases with higher incident energies.

IV. SUMMARY

We studied the application of the DEA method for a wide energy range. We studied the angular distributions of elastic scattering of ^{8}B, ^{9}C, and ^{11}Be on ^{208}Pb at incident energies of approximately 10 to 60 MeV/nucleon. We compared the CDCC and DEA methods for the angular distributions of elastic scattering. Our results show the difficulty of properly describing the elastic scattering for the low-energy case within the DEA method. However, we found that an empirical correction significantly enhances the method's ability to reproduce the Coulomb deflection, which was previously identified as a missing component of DEA. With this correction, the agreement between the DEA and CDCC results is markedly improved. Moreover, DEA using the empirical correction also shows good agreement with experimental data. We also studied the effect of relativistic kinematics corrections on the angular distributions of elastic scattering for ^{8}B on ^{208}Pb at incident energies ranging from 20 to 60 MeV/nucleon. We examined the effects of relativistic corrections on these angular distributions. Our calculations reveal that relativistic corrections play a crucial role in accurately describing the angular distributions of elastic scattering, even at relatively low incident energies of approximately 40 MeV/nucleon. From these results, we conclude that DEA including the empirical and relativistic corrections can provide an efficient alternative tool to describe the elastic scattering of weakly-bound nuclei within a wide energy region. To extend the DEA method to the high regions of incident energies up to around 1 GeV/nucleon, a suitable phenomenological potential for reactions in the high energy region is important. We plan to study this in future work.

References

[1] I. Tanihata, H. Hamagaki, O. Hashimoto *et al.*, Phys. Rev. Lett. **55**, 2676 (1985)

[2] A. S. Jensen, K. Riisager, D. V. Fedorov *et al.*, Rev. Mod. Phys. **76**, 215 (2004)

[3] R. Kanungo, W. Horiuchi, G. Hagen *et al.*, Phys. Rev. Lett. **117**, 102501 (2016)

[4] A. Ozawa, T. Kobayashi, T. Suzuki *et al.*, Phys. Rev. Lett. **84**, 5493 (2000)

[5] R. Kanungo, C. Nociforo, A. Prochazka *et al.*, Phys. Rev. Lett. **102**, 152501 (2009)

[6] D. Steppenbeck, S. Takeuchi, N. Aoi *et al.*, Nature **502**, 207 (2013)

[7] M. Rosenbusch, P. Ascher, D. Atanasov *et al.*, Phys. Rev. Lett. **114**, 202501 (2015)

[8] Kris Heyde and John L. Wood, Rev. Mod. Phys. **83**, 1467 (2011)

[9] X. F. Yang, C. Wraith, L. Xie *et al*., Phys. Rev. Lett. **116**, 182502 (2016)
[10] J. J. Kolata, V. Guimarães, and E. F. Aguilera, Eur. Phys. J. A **52**, 123 (2016)
[11] O. R. Kakuee, M. A. G. Alvarez, M. V. Andrés *et al*., Nucl. Phys. A **765**(3), 294 (2006)
[12] K. Rusek, N. Keeley, K. W. Kemper *et al*., Phys. Rev. C **67**, 041604 (2003)
[13] A. M. Sánchez-Benítez, D. Escrig, M. A. G. Álvarez *et al*., Nucl. Phys. A **803**(1), 30 (2008)
[14] Y. Y. Yang, X. Liu, and D. Y. Pang, Phys. Rev. C **94**, 034614 (2016)
[15] F. F. Duan, Y.Y. Yang, K. Wang *et al*., Phys. Lett. B **811**, 135942 (2020)
[16] Y. Y. Yang, X. Liu, D. Y. Pang *et al*., Phys. Rev. C **98**, 044608 (2018)
[17] N. Austern, Y. Iseri, M. Kamimura, M. Kawai *et al*., Physics Reports **154**(3), 125 (1987)
[18] J. A. Tostevin, F. M. Nunes, and I. J. Thompson, Phys. Rev. C **63**, 024617 (2001)
[19] M. Avrigeanu and A. M. Moro, Phys. Rev. C **82**, 037601 (2010)
[20] Y. Kucuk and A. M. Moro, Phys. Rev. C **86**, 034601 (2012)
[21] Y. P. Xu and D. Y. Pang, Phys. Rev. C **87**, 044605 (2013)
[22] R. J. Glauber, *Lectures on Theoretical Physics* Vol. 1 (New York: Interscience, 1959), p.315
[23] K. Yabana Y. Suzuki, R. G. Lovas and K. Varga, *Structure and Reactions of Light Exotic Nuclei* (London: CRC Press, 2003), p. 315.
[24] P. Capel, H. Esbensen, and F. M. Nunes, Phys. Rev. C **85**, 044604 (2012)
[25] T. Fukui, K. Ogata, and P. Capel, Phys. Rev. C **90**, 034617 (2014)
[26] G. Goldstein, D. Baye, and P. Capel, Phys. Rev. C **73**, 024602 (2006)
[27] C. A. Bertulani and P. Danielewicz, *Introduction to Nuclear Reactions* (Boca Raton: CRC Press, 2004), p.515
[28] C. A. Bertulani, C. M. Campbell, and T. Glasmacher, Comput. Phys. Commun. **152**(3), 317 (2003)
[29] W. J. Satchler, G. R. R. L. Varner, Nucl. Phys. A. **540**(1), 533 (1992)
[30] H. Esbensen and G. F. Bertsch, Nucl. Phys. A **600**(1), 37 (1996)
[31] P. Capel, R. C. Johnson, and F. Nunes, Phys. Lett. B705 (2011)
[32] P. Capel, R. C. Johnson, and F. M. Nunes, Phys. Rev. C **88**, 044602 (2013)
[33] P. Capel, D. Baye, and V. S. Melezhik, Phys. Rev. C **68**, 014612 (2003)
[34] X. Y. Yun, F. Colomer, D. Y. Pang *et al*., J. Phys. G: Nucl. Part. Phys. **46**(10), 105111 (2019)
[35] R. L. Varner, W. J. Thompson, T. L. McAbee *et al*., Phys. Rep. **201**(2), 57 (1991)
[36] Y. Y. Yang, J. S. Wang, Q. Wang *et al*., Phys. Rev. C **87**, 044613 (2013)